Mode I Translaminar Fracture Toughness of High Performance Laminated Biocomposites Reinforced by Sisal Fibers: Accurate Measurement Approach and Lay-up Effects

Francesco Bongiorno, Carmelo Militello*, Bernardo Zuccarello

University of Palermo - Department of Engineering, Viale delle Scienze, 90128 – Palermo, Italy.

** Corresponding author email: carmelo.militello01@unipa.it*

ABSTRACT

The present work performs a systematic experimental analysis of the translaminar fracture behavior of high performance biocomposites constituted by green epoxy reinforced by sisal fibers, by varying the main influence parameters as fiber concentration and lay-up. Despite the corrective function properly introduced to take into account the anisotropy as well as the use of the equivalent crack length, the study shows that the LEFM does not give accurate estimations of the fracture toughness, because the extension of the near tip damaged zone is higher than the singular dominated one. Accurate estimations can be obtained instead by the proposed modified area method that takes into account both the local damage and the fiber bridging that occurs during crack propagation, that lead to *R*-curves whose asymptotic values constitute the true fracture toughness of the biocomposites examined. The constancy of the damage mechanisms observed by varying the fiber concentration, allows the user to compute the fracture toughness of a generic laminate from the specific fracture energy of the unidirectional lamina. Finally, the relatively high fracture toughness of the examined laminates allows to state that they can advantageously replace not only other composites having lower toughness, but also metals as steel, aluminum and titanium.

keywords: A. Bio composites, A. Natural fibre composites, B. Fracture toughness, Translaminar failure, R-curves.

1. INTRODUCTION

The increasing focus on environmental issues has led to a recent interest in the eco-sustainable, eco-compatible and renewable materials. Among these, an important role is played by the so-called biocomposites, materials generally made of polymer matrices with low environmental impact, reinforced by natural fibers, characterized by very low density, usually less than 14 kN/m^3 [1–3]. A considerable research activity on the mechanical properties (static and dynamic) of these biocomposites laminates under different loading condition (tensile, bending, compression, etc.), has been reported in the literature and also reliable models of micromechanics, have been implemented.

However, to date only many research works have been devoted to the delamination [4] whereas only a few studies have been focused on the fracture behavior of these materials, especially with reference to

the so-called translaminar fracture [5] that occurs when the failure mechanism simultaneously involves all the laminae with a forward face of the crack that crosses the entire thickness.

However, it is a common opinion of the most researchers [6] that, with the improvement of the delamination strength of the modern composites, the translaminar fracture resistance will play an increasingly important role.

Mode I translaminar fracture strength (toughness) is classically defined as the specific energy absorbed by the material for the formation of a unitary fracture surface associated with the mode I propagation of a crack, that macroscopically affects the composite laminate throughout its thickness. Due to the intrinsic heterogeneous and non-isotropic nature of composite materials, the analysis of fracture toughness is clearly more complex than traditional homogeneous and isotropic materials; for a fixed matrix type, it is affected in fact by several parameters as reinforcement type, orientation, laminate lay-up and the fiber volume fraction. Consequently, it generally needs specific experimental investigations [7–13] aimed to the estimation of the well-known critical *stress intensity factor* K_{Ic} in accordance with the Linear Elastic Fracture Mechanics (LEFM) or, alternatively, the evaluation of the *critical strain energy release rate* G_{Ic}.

In brief, the literature shows that the fracture strength of synthetical long fiber laminates (CFRP and/or glass/carbon hybrids with thermoplastic or thermoset matrices) have been widely studied [11–20], also by considering the effect of temperature, constraint and notch tip radius. In summary, such studied have highlighted that the fracture performance is governed by the fibers failure of the laminae orthogonal to the crack axis, and the influence of temperature and radius crack tip are generally low; the influence of the anisotropy and the geometry of the specimens [16], can significantly limit the usual extension to the composites of the approaches and standards proposed for homogeneous and isotropic materials.

More recent studies [21,22] have considered also short-fibre composite laminates manufactured by additive processes using green matrix (PLA); they have shown that such composites exhibits appreciable increments of the fracture toughness compared to that of the matrix alone [21].

With refer to the computational methods that can be applied to the analysis of the translaminar fracture toughness, several researches [8,23–26] have provided important indications about the best technique in terms of reliability and reproducibility, whereas other researches [27–30] have presented the so called fracture resistance curve (*R*-curve) that describe the intimate behavior of composites during fracture. In more detail, in [15,31–33] the effects of the main laminate parameters (dimension, thickness etc.) and of the damage processes near the crack tip, have been studied.

Recent studies [34] have also considered the effects of the strain speed by evaluating the dynamic *R* curves that, as it is expected, have shown beneficial increments of the toughness with speed.

Among the first fracture studies carried out by considering biocomposites reinforced with natural fibers, worthy of mention is the work [35] that has analyzed the behavior of sisal fiber polymer mortar composites, highlighting the positive effects of the fiber volume fraction and the negative effects of the mercerization with NaOH.

Interesting studies have been carried out recently on biocomposites [36–38] constituted by epoxy reinforced with natural fibres (bamboo, cotton, flax etc.); they have investigated also the influence of the fiber direction [38] on the crack propagation path, highlighting also that the speed of the crack propagation in the direction of the fibers increases significantly with V_f.

In order to give a contribution to the knowledge of intralaminar fracture behavior of interesting high performance biocomposite laminates (tensile strength of about 500 MPa) consisting of green epoxy matrix reinforced with optimized long sisal fibers [39–45], systematic experimental tests have been carried out by means of CT specimens, supported by appropriate FEM simulations. Particular attention has been paid other than to the influence of the fiber volume fraction and laminate lay-up, also to the local material damage that occurs near the crack tip as well as to the appreciable fiber bridging phenomena that lead to fracture resistance *R*-curves characterized by steady-state values very higher than the initial fracture toughness.

2. MATERIALS AND METHODS

As mentioned above, the high performance biocomposites examined in this paper consist of green epoxy matrix reinforced by optimized sisal fibers. The following sections describe briefly the mechanical properties of fibers and matrix, as well as the manufacturing process used to obtain the different biocomposite laminates (unidirectional, cross-ply, braided and quasi-isotropic, each with V_f =0.35 and 0.70) and the test method used their fracture characterization.

2.1 Optimized sisal fibres

The sisal fibers used in the present work, are structural fibers extracted from the perimeter of medium third of mature leaves. In order to maintain a high degree of renewability, the fibres were subjected only to a manual cleaning and subsequent drying process, without any surface treatment. Tab.1 shows the specific weight ρ_f along with the mechanical properties of the fiber batch used in this work, such as longitudinal tensile strength $\sigma_{f,R}$, longitudinal Young modulus E_f, and tensile failure strain $\varepsilon_{f,R}$, obtained by single-fibre tensile tests performed in accordance with ASTM [46]; for more details the reader can see also refs. [41,42].

Table 1 Properties of the sisal fibers considerate in the present study.

Material	$\boldsymbol{\rho_f}$ [g/cm^3]	$\boldsymbol{\sigma_{f,R}}$ [MPa]	$\boldsymbol{E_f}$ [MPa]	$\boldsymbol{\varepsilon_{f,R}}$ [%]
Agave Sisalana (sisal)	1.45	690	40250	1.76

Using such fibers, unidirectional “stitched” fabrics were preliminary obtained in laboratory by a manufacturing process consisting into: (a) manual stretching of the fibers in order to eliminate natural undulations, (b) alignment of the straight fibers arranged into small groups (see Fig.1a) and (c) transversal stitching by using an automatic machine. Fabrics with a weight of about 220 g/m^2 have been so obtained (see Fig.1b).

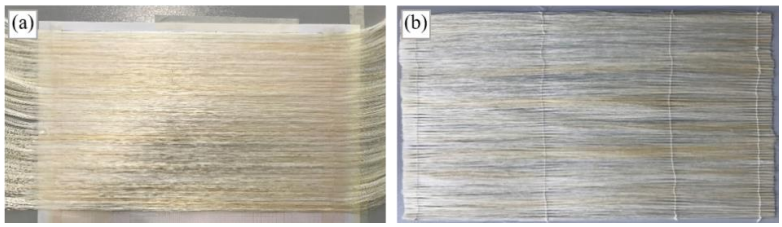

Figure 1 (a) stretched and aligned fibers, (b) unidirectional "stitched" fabrics obtained in laboratory.

2.2 Green matrix

A green epoxy resin (*partial biobased epoxy*), produced by American Entropy Resin Inc. (San Antonio, CA, USA), named SUPERSAP CNR, with IHN-type hardener [47], has been used as matrix. It is in practice an epoxy resin obtained by an ecofriendly manufacturing process through green chemistry, sustainable raw materials, and efficient manufacturing conserving energy, minimizing harmful by products and reducing greenhouse gas emissions of resins and hardeners.

As widely shown in previous studies by the same authors [39–45], this matrix exhibits an almost elastic linear behavior; the main characteristics, such as density ρ_m, tensile strength $\sigma_{m,R}$, Young modulus E_m, and tensile failure strain $\varepsilon_{m,R}$, are reported in Tab.2.

Table 2 Properties of the green epoxy resin, used as matrix [47].

Material	ρ_m [g/cm^3]	$\sigma_{m,R}$ [MPa]	E_m [MPa]	$\tau_{m,R}$ [MPa]	$\varepsilon_{m,R}$ [%]
Green epoxy	1.05	50	2500	35	2.5

2.3 Manufacture of biocomposite laminates

The various laminates have been manufactured by hand lay-up carried out inside a suitable mould. To obtain high quality laminates (without voids and/or defects), after an appropriate time of partial gelification, the laminate is subjected to a compression-moulding process, using a press of 100 tons for 24 hours. In order to optimize the mechanical properties, each laminate has been subjected to a subsequent thermo-mechanical cure process by using the optimized time laws $T(t)$ and $p(t)$ described in [41,42].

The following Tab.3 lists the 8 biocomposite laminates so obtained: 4 different lay-ups (unidirectional UD, cross-ply CP, braided-ply BP, and quasi-isotropic QI) and two distinct fibres volume fraction V_f (equal 35% and 70%) for each lay-up, in order to encompass in practice the generic laminate potentially used for structural and semi-structural applications.

Table 3 Lay-up and fiber volume fraction of the various biocomposites considered.

Laminate	**Denomination**	V_f [%]	**Lay-up**
Unidirectional	UD35	35	$[0]_8$
	UD70	70	$[0]_{16}$
Cross-ply	CP35	35	$[(0/90)_2]_S$
	CP70	70	$[(0/90)_4]_S$
Braided-ply	BP35	35	$[(+45/-45)_2]_S$
	BP70	70	$[(+45/-45)_4]_S$
Quasi-isotropic	QI35	35	$[(0/+45/-45/90)]_S$
	QI70	70	$[(0/+45/-45/90)_2]_S$

For all the laminates, the number of laminae (8 for V_f =35% and 16 for V_f =70%) have been selected in order to obtain a thickness of 3 mm, that is superior than the lower limit described by the ASTM E1922 standard [48], equal to about 2 mm.

As an example, the following Fig.2 shows the images of 4 laminate panels type UD70, CP70, BP70 and QI70.

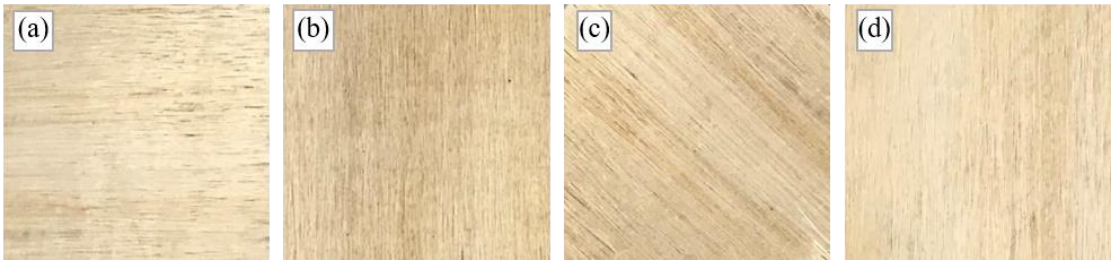

Figure 2 Laminates type (a) UD70, (b) CP70, (c) BP70 e (d) QI70 obtained by compression-moulding.

2.4 Test method and experimental setup

All the experimental fracture tests have been carried out by using the compact tension (CT) configuration considered by the ASTM E399 [49], E1820 [50] and D5045 [51] standards. As it is well known, CT specimens are the most used for the translaminar fracture analysis of composites [8,14,19,20,23,30,52], because in general it assure the stable crack growth that is necessary to relieve both the initial toughness and the characteristic resistance *R*-curves. However, the experimental test have been carried out by considering also the main rules contained into the ASTM E1922 standard [48] that refers specifically to the translaminar fracture test of biocomposite laminates. From each of the 8 biocomposite laminate panels manufactured, 5 CT specimens were cut, obtaining a total of 40 specimens. In accordance with the ASTM E1922 [48] such a specimens number have assured to obtain three valid replicate test results for each laminate considered.

The geometry of the specimens, described in [51], is reported in detail in Fig.3a; as an example, Fig.3b shown the image of a specimen CP70. In accordance with the ASTM standard, the first part of the crack (having length of 30 mm) have obtained through a circular saw blade of 4 mm thickness, whereas the second part adjacent to the tip (having length of 10 mm) have obtained with a special razor saw blade of about 0.2 mm thickness.

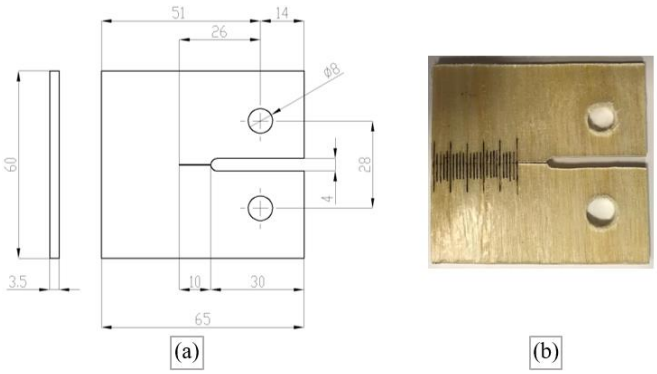

Figure 3 (a) sketch of the CT specimen and (b) relative specimen type CP70.

As shown in Fig.3b, a proper graduated scale have been engraved on each specimen in order to measure the crack growth by simple photographic observations.

All the translaminar fracture tests have been carried out by using an INSTRON 3367 testing machine equipped with 30 kN load cell. Each specimen has been instrumented by a notch-mouth displacement gage type INSTRON 2670, and has been loaded under displacement control at a rate of 0.5 mm/min, that assure the fulfillment of the time limit of 100 s to reach the peak load, prescribed by the ASTM E1922 [48]. The growth crack, has been monitored by a NIKON D5100 camera with AF-S VR Dx 18-55 mm lens that allows multiple shots with a constant frequency of 1 Hz, that allow to register the crack growth with an actual spatial resolution of at least 0.033 mm.

3. EXPERIMENTAL RESULTS

Firstly, the experimental evidence has shown that the fracture mode of biocomposite laminates with V_f =35% are practically identical to those observed for the laminates with V_f=70%. Therefore, in order to detect preliminarily that in all the considered lay-up (UD, CP, BP and QI) the actual fracture mode is the expected mode I, Fig.4 shows the images of 4 different biocomposite specimens with V_f=70%, during fracture test, along with a zoom of the relative fracture surfaces after test.

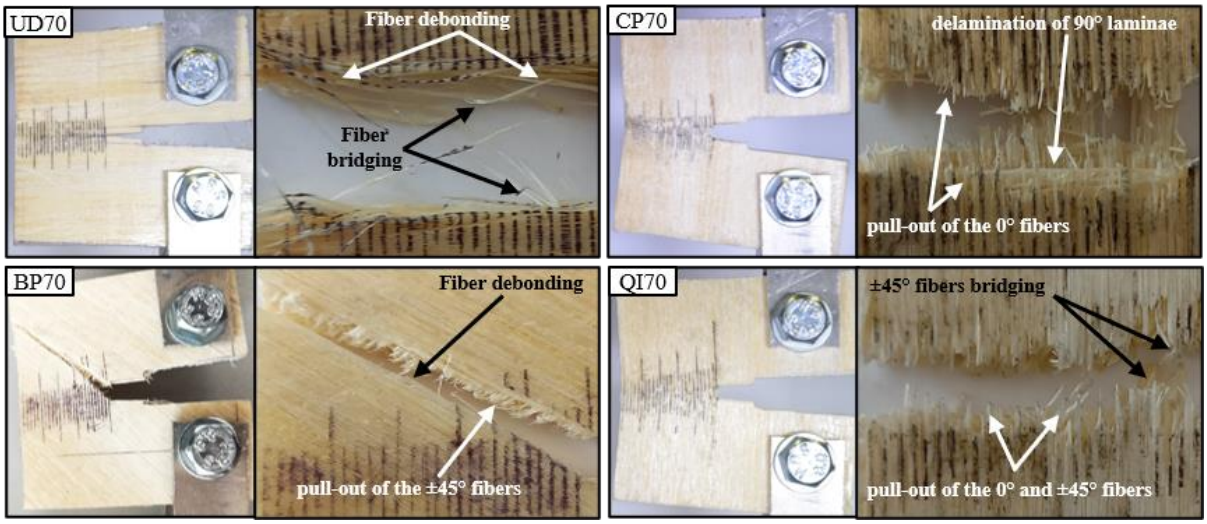

Figure 4 Specimens with V_f =70% during test and zoom of the relative fracture surfaces after test.

The analysis of Fig.4 shows clearly that in the UD, CP and QI laminates the crack propagates perpendicularly to the applied load, i.e. in the expected mode I, whereas in the BP laminates the crack propagates in the direction of 45°, i.e. in a mixed mode I + II. This particular direction of crack propagation is in accordance with the general rule that the actual crack propagation path is that associated with the minimum fracture energy. In this case, in fact, the propagation in pure mode I would involve the fracture of all the fibers of the laminate, whereas the crack propagation at +45° (or, alternatively, at -45°) involves only the fracture of the 50% of the fibers, with a consequent significant reduction of the propagation energy.

Taking into account that the experimental evidences has shown that in the QI laminates the laminae oriented at ±45° failure always according to mode I, i.e. with fracture surface orthogonally to the applied load, it follows that the fracture tests performed on the BP specimens are meaningless so that they will not be considered in the following, and the contribution to the fracture toughness of a generic angle-play laminate given by the laminae at ±45° will be estimated through proper energetic considerations.

The observation of the damage mechanisms shows in particular that in the UD laminates (fibers axis orthogonal to the load direction) the fracture propagates in practice in the inter-fiber space, essentially within the matrix, although it involves also modest fiber-bridging (that increases with V_f) and consequent debonding of the fibers having alignment errors (see Fig.4). The primary intralaminar delamination mechanism within the matrix, justifies the low fracture load values observed for this lay-up (always less than 150 N).

Considering the CP laminates instead, it is observed that the crack propagates with negligible local deviations (twisting of some millimeters) with respect to the mode I, involving the tensile failure of the fibers of the laminae at 0° and then their successive secondary pull-out, as well as the intra-laminar delamination of the laminae at 90° (see Fig.4). Also, limited phenomena of partial interlaminar delamination are observed around the fracture surface, i.e. in the near tip damaged zone (N-TDZ).

Finally, considering the QI laminates, the damage mechanisms observed for each type of laminae are essentially: tensile failure of fibers and matrix of the lamina at 0°, intralaminar delamination failure on the matrix and fiber/matrix debonding for the lamina at 90°, and shear failure of fibers and matrix of the laminae at ±45° (see Fig.4). In detail, the observation of the crack growth process shows how the QI exhibits also limited effects of secondary pull-out on the laminae at 0°, as it has been observed in the CP laminates, as well as the limited effects of fiber-bridging in the laminae at 90° already observed in the UD laminates and, above all, significant phenomena of fiber-bridging related essentially to the rotation (sliding) of the laminae at ±45°.

Finally, the experimental evidence have shown that in all the cases, for crack length higher than 40-42 mm, phenomena of elastic out-of-plane buckling due to the small specimen thickness (3 mm) and the high compressive stresses on the resistance section opposite the crack tip, are observed. Such phenomena lead to significantly decreasing of the specimen compliance, without any further crack growth. Consequently, the fracture test become invalid for $a > 42$ mm; for this reason all the calculations presented below are always limited to this value of the crack length. It is noticeable to note that such out-of-plane buckling phenomena and the consequent limitation, are considered also by the ASTM E1922 standard [48] for the extended compact tension specimen considered.

The following Fig.5 shows the average fracture curves of the UD, CP and QI specimens with V_f=35% and 70%:

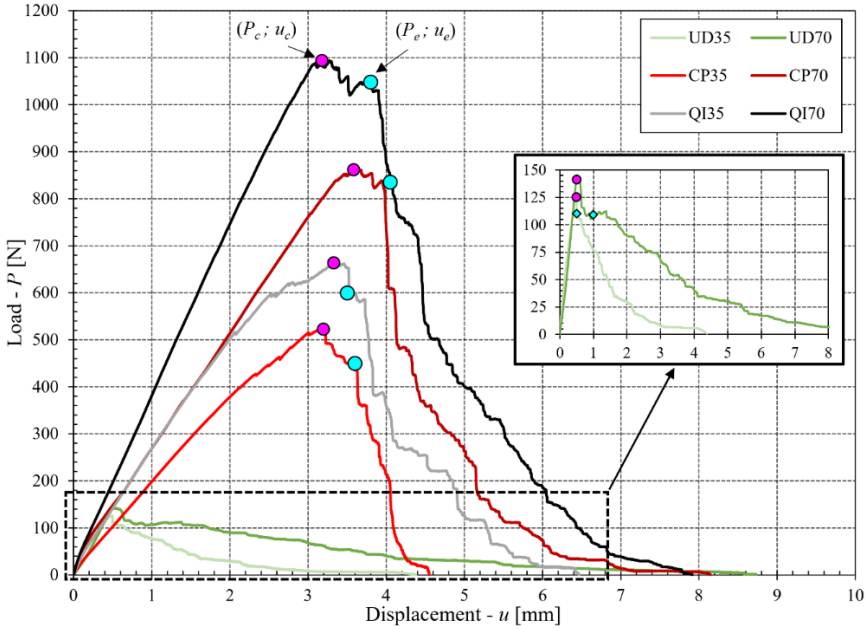

Figure 5 Mean fracture curves of the various biocomposite laminates considered.

The examination of Fig.5 shows how, for any lay-up and any V_f value, the generic fracture curve is always constituted by a first linear elastic segment that extends up to applied load values always higher than 75% the maximum load (critical) supported by the specimen; this first phase is followed by a second increasing part characterized by an appreciable and progressive stiffness decrement, which corresponds to progressive damage of the N-TDZ. However, singular are the curves related to UD biocomposites that exhibit a higher linearity, as well as a slight decreasing stiffness with fibers concentration, due to the high anisotropy of the sisal fibers characterized by transversal Young modulus lower than the matrix one [53].

In terms of initial fracture toughness, represented in practice by the critical load P_c (maximum load supported by the specimen at the incipient crack growth condition), the examination of Fig.5 shows that, as expected, it always increases significantly with V_f indicating that the fracture of the biocomposites examined is essentially dominated by the fiber failure. In more detail, for UD laminates the increment of critical load is rather modest (+13%) since, as already observed in Fig.4, the fracture process involves primary the matrix delamination and is only marginally affected by the fibers through limited fiber-bridging effects. More significant is the effect of V_f for angle-ply laminates: passing from V_f =35% to V_f =70% P_c increases by about 65% for CP and QI. However, it is noted that although the fibre concentration doubles, the critical load does not double; this is due to the greater extension of N-TDZ in the biocomposites having V_f =35%, corresponding to the higher deviations from the linearity of the fracture curve segments that precede the critical load (see CP35 and QI35 curves in Fig.5), and to the consequent positive effects (the local material damage of the composite works similar to the plasticity of the isotropic metallic materials) on fracture toughness. Also, very significant variations of the peak load are related to the lay-up: as an example for V_f =70, moving from the UD lay-up characterized by primary intralaminar delamination associated with limited fiber-bridging effects, to the CP lay-up

characterized by the tensile fiber failure of the 0° laminae along with secondary pull-out effects, to the QI lay-up characterized also by additional shear fiber failure of the ±45° lamine mixed to beneficial phenomena of fiber bridging, it moves from about 139 N, to about 860 N (increment of +600% approximately), to about 1100 N (further +30% approximately).

Finally, the experimental evidences shows that for all the biocomposites examined the critical load is always followed by an almost stable crack propagation (see Fig.5), that lead to the complete specimen failure for displacements of the applied load that varies from about 4.5 mm (for CP35) to about 8 mm (for CP70).

Although the criterion expressed by Eq.2 of the ASTM E1922 standard [48] relative to the maximum notch-mouth deviation is generally verified for the analyzed biocomposites, the relatively low strength with respect to the synthetical fibers composites indicate the possible existence of a relatively large extension of the N-TDZ relative to the maximum notch-mouth deviation is generally verified for the analyzed biocomposites, the relatively low strength with respect to the synthetical fibers composites indicate the possible existence of a relatively large extension of the N-TDZ and consequently that:

(a) the application of LEFM may subjected to practical limitations if the N-TDZ dimensions are greater than the dimensions of the so called singularity dominated zone (SDZ); in other words, the actual stress distribution near the crack tip becomes very different to the theoretical one governed by the SIF K_I, which loses all meaning. Although, in fact, the ASTM E1922 standard subordinate generically the validity of the LEFM to the condition in which the N-TDZ dimensions are small compared to the notch length or the in-plane specimen dimension, in principle its validity decays if the damaged zone is wider than the SDZ.

(b) the correct analysis of K_{Ic} or, alternatively, of the critical strain energy release rate G_{Ic}, shall be performed by replacing the critical nominal length a detected visually, with the so called equivalent crack length a_{eq}, that allow to take into account the effect of the N-TDZ; as already amply demonstrated in literature [4,5], this equivalent crack length can be accurately determined from the measurement of the effective current compliance of the specimen $C = (u / P)$, by using the curve $C(a)$ obtained preliminary by experimental investigations (or by accurate numerical simulations) by varying the length of the crack of the test piece CT.

4. EVALUATION OF COMPLIANCE, EQUIVALENT CRACK LENGTH AND SDZ EXTENSION

4.1 Evaluation of the compliance curve

For each biocomposite examined, the relative $C(a)$ curve has been determined experimentally by measuring the ratio (u/P) for different crack lengths included between 20 mm to 42 mm (higher crack length have not been considered due to the above described out-of-plane buckling phenomena). In detail, in order to ensure the absence of significant damage of the material near the crack tip ($a_{eq} = a$), a load P equal to about 0.25 times the peak load has been applied. Also, the required crack length have been

always obtained accurately with the appropriate cut of the specimen with hacksaw. The experimental results thus obtained for the different laminates are reported in the following Fig.6.

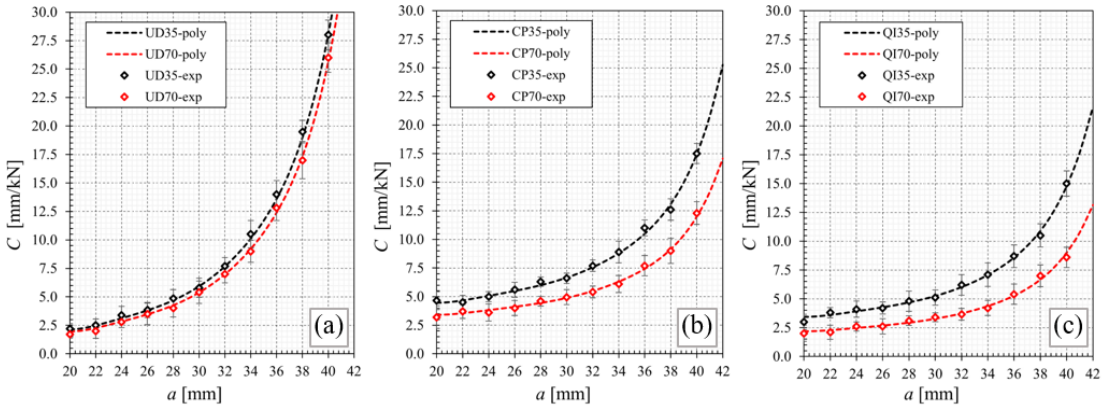

Figure 6 Compliance curves obtained experimentally for the (a) UD, (b) CP and (c) QI biocomposite laminates having V_f =35% and 70%.

The analysis of the experimental data have shown that they can be approximated with simple six order polynomials, i.e.:

$$C(a) = c_0 + c_1 a + c_2 a^2 + c_3 a^3 + c_4 a^4 + c_5 a^5 + c_6 a^6 \qquad (1)$$

Such polynomials provide accurate continuous expression not only of the curves $C(a)$ but also of their derivative dC/da involved in some energetic methods; such approximations are always more accurate than those provided by the functions used by Laffan et al.[6,20]. For each examined laminate the values of the coefficients of Eq.1 have been evaluated.

4.2 Evaluation of the equivalent crack length

As soon as the critical value C_c of the actual compliance of the generic specimen subjected to the critical load P_c (condition of incipient crack propagation) is computed by the ratio:

$$C_c = \frac{u_C}{P_c} \qquad (2)$$

the use of the corresponding polynomial represented by the Eq.1 allows, by iterative resolvent procedure, the immediate evaluation of $a_{eq}(P_c)$ and of the difference $a_{eq}(P_c)$ - $a_{nom}(P_c)$, being in this case a_{nom} = 26 mm. Obviously, this increment of the crack length constitutes an underestimation of the initial size of the N-TDZ (the material inside N-TDZ is in not completely damaged). For each biocomposite examined, the values of C_c, $a_{eq}(P_c)$ and $a_{eq}(P_c)$ - $a_{nom}(P_c)$ are given in the following Tab.4:

Table 4 Values of C_c, a_{eq} and (a_{eq} - a_{nom}) for the various examined biocomposites.

Laminate	**Denomination**	C_C [mm/kN]	$a_{eq}(P_c)$ [mm]	$a_{eq}(P_c)$ - $a_{nom}(P_c)$ [mm]
Unidirectional	UD35	3.95	26.32	0.32
	UD70	3.56	26.24	0.24
Cross-ply	CP35	6.12	28.42	2.42
	CP70	4.16	26.37	0.37
Quasi-isotropic	QI35	5.02	29.30	3.30
	QI70	2.91	27.79	1.79

The analysis of Tab.4 shows that for UD laminates the crack length increment ($a_{eq} - a_{nom}$) is relatively modest, and comparable with the inter-fiber space dimensions. Relatively higher are instead the values for CP laminates (2.42 mm and 0.37 mm for V_f =30% and V_f =70%, respectively) and QI (3.30 and 1.79 mm for V_f =30% and V_f =70%, respectively). For any biocomposite, as expected, such crack increment decreases if V_f increases, because the brittleness of the biocomposites increase with V_f.

In the following Fig.7 the values of a_{eq} that occur during the crack growth, are plotted against the nominal values a_{nom} relieved experimentally by the camera.

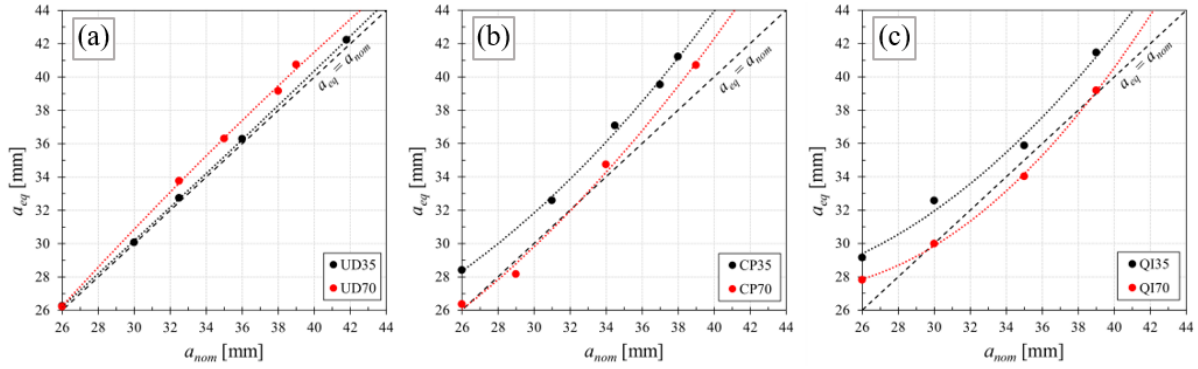

Figure 7 Comparison between a_{eq} and the corresponding value a_{nom} for the various examined biocomposites.

The analysis of Fig.7a shows that for the UD laminates the difference a_{eq} - a_{nom} is appreciable only for V_f = 70%; also it increases monotonically with the crack length; for CP and QI laminates, instead, it decreases due to the progressive fiber bridging phenomena that lead to a reduction of the dimension of the N-TDZ. In more detail, it is seen an initial reduction of a_{eq} followed by an increase for values of a_{nom} ≥34 mm, due to the reduction of the fiber bridging caused by the increase of the crack opening angle, as well as to the increase of the out-of-plane buckling of the resistant section of the specimens.

4.3 Evaluation of the SDZ extension

In order to verify the applicability of the LEFM, the typical size of the SDZ that occur in the CT specimens has been evaluated by comparing the actual normal stress distribution given by accurate FEM simulations, with the theoretical one predicted by the singular term provided by the Theory of Elasticity [4,5]. As an example, in the following Fig.8 the distribution of the stress normal to the axis of the crack (opening stress) obtained by means of accurate FEM simulations of the laminate QI70, is compared with the distribution of the same stress given by the theory of elasticity:

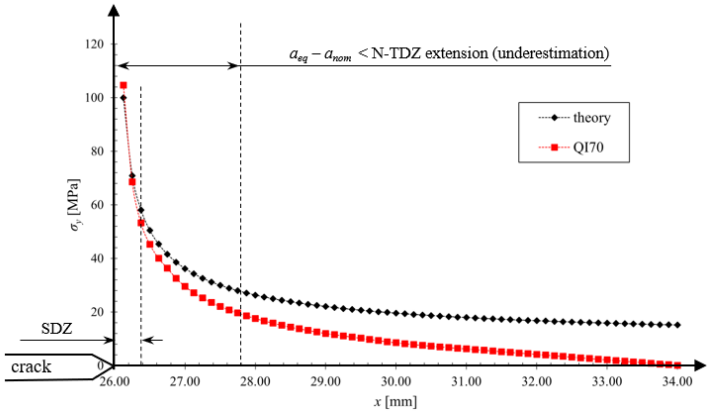

Figure 8 Comparison between the actual opening stress σ_y computed by FEM and the theoretical one for the QI70 biocomposite examined.

From Fig.8 it is seen that the extension of the SDZ, equal to approximately 0.4 mm, is significantly less than the difference $a_{eq}(P_c)$ - $a_{nom}(P_c)$ that in this case assumes the value of 1.79 mm (see Tab.4); consequently, taking into account that the extension of the N-TDZ is certainly superior to such difference, it can be stated that for QI70 biocomposites K_{Ic} cannot be rigorously used for the characterization of its fracture toughness which, alternatively, can be more accurately evaluated by using energetic approaches based on the G_{Ic}. Similar results are obtained for CP35 and QI35 laminates that have values of $a_{eq}(P_c)$ - $a_{nom}(P_c)$ equal to 2.42 mm and 3.30 m respectively (see Tab.4). However, in the following the LEFM approach will be used the same for the estimation of the fracture toughness of all biocomposites, together with appropriate alternative energetic approaches, in order to evaluate the magnitude of the actual errors affecting the fracture toughness evaluation by using K_{Ic} .

5. DATA REDUCTION

The evaluation of the fracture toughness of the examined biocomposites have been carried out by using (a) the LEFM approach described by the ASTM E399 standard [49], as well as by the most used methods for composite materials, as the so called *Area Method* (AM) and the *Compliance Calibration* (CC) [23].

5.1 LEFM approach

For the CT specimens the SIF K_{Ic} that governs the stress state near the crack tip is expressed by the following formula [49,51]:

$$K_{Ic} = \frac{P_c}{t\sqrt{W}} f(a/W) \tag{3}$$

where P_c is the measured critical load that causes fracture propagation, t is the specimen thickness, W is the distance from the point of application of the load (hole center) to the opposite end of the specimen, a is the initial crack length measured from the line of application of the load (see Fig.3a), and $f(a/W)$ is the well-known weight function which takes into account the geometry of the specimens and the specific loading conditions (eccentric traction of the test piece CT), given by the same ASTM standards [49,51]:

$$f(a/W) = \frac{(2 + a/W)[0.886 + 4.64(a/W) - 13.32(a/W)^2 + 14.72(a/W)^3 - 5.6.(a/W)^4]}{(1 - a/W)^{1.5}} \tag{4}$$

Eq.3 is strictly valid only for isotropic materials, although several authors [16,23,30] have extended its application to orthotropic materials (composites, etc.) disregarding the effects of anisotropy of the material. The application of Eq.3 to an orthotropic material, such as the examined biocomposites, therefore needs the introduction of a correction factor C_{anis} which takes into account the anisotropy of the material that influences the actual stress distribution around the crack tip (and then the K_{Ic} value), by re-written Eq.3 as:

$$K'_{Ic} = \frac{P_c}{t\sqrt{W}} f(a/W)\, C_{anis} \tag{5}$$

In the usual plane stress condition that occurs in composite laminates, this C_{anis} correction coefficient is in practice related to the laminate orthotropy through the orthotropic ratios R_E and R_G given by:

$$R_E = \frac{E_L}{E_T} \qquad R_G = \frac{2G_{LT}(1+\nu_{LT})}{E_L} \qquad (6, 7)$$

In order to obtain an accurate estimation of the proposed corrective function $C_{anis} = f(R_E, R_G)$, accurate FEM simulations of CT specimens have been performed by considering several orthotropic laminates having various orthotropic ratios R_E and R_G properly chosen to describe in practice all the plane domain defined by such ratios for fibre-reinforced composites of practical application. Dividing the K_{Ic} value numerically evaluated (corrected value) with that provided by Eq.3 (isotropic value) with the same load applied, the C_{anis} values corresponding to each considered pair (R_E, R_G), have been obtained.

These values are well approximated by the complete second-degree polynomial represented in the following Fig.9:

This polynomial has the following simple analytical expression:

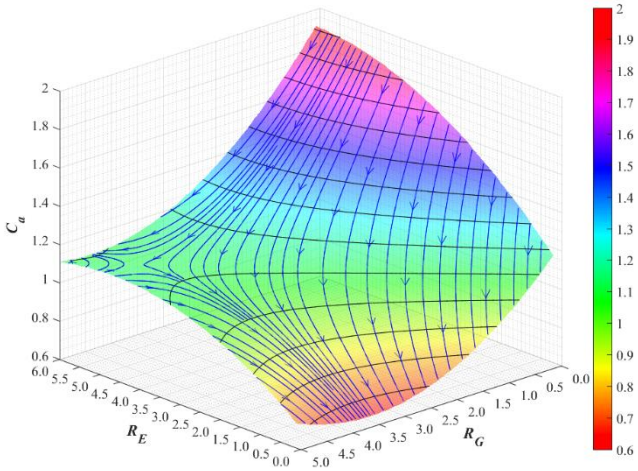

Figure 9 Correction coefficient C_{anis} versus the two anisotropic ratios R_E and R_G.

$$C_{anis} = 1.177 + 0.2363\,R_E - 0.2987\,R_G - 0.01895\,{R_E}^2 - 0.01186\,R_E R_G + 0.04178\,{R_G}^2 \qquad (8)$$

It is seen how this corrective coefficient takes in practice significant values included between 0.6 and 2, so that it possible to state that if the material anisotropy is neglected than coarse approximations in the estimation of K_{Ic} are given by the simple use of Eq.3 provided by the ASTM E399 standard [49]. In particular, for the biocomposite laminates examined, Eq.8 provides the values of the correction coefficient reported in the following Tab.5:

Table 5 Coefficient C_{anis} for the biocomposites examined.

Laminate	Denomination	C_{anis}
Unidirectional	UD35	0.907
	UD70	0.801
Cross-ply	CP35	1.318
	CP70	1.389
Quasi-isotropic	QI35	1.082
	QI70	1.082

Tab.5 shows that, as it is expected, this correction coefficient is close to 1 for QI laminates (behavior close to that of an isotropic material), less than one for UD laminates with longitudinal axis aligned with the crack (fibers orthogonal to the load and notch coefficient lower than the isotropic one), and

significantly higher than one for CP laminates (fibers parallel to the load and notch coefficients higher than the isotropic one).

From the K_{Ic} values approximately evaluated by Eq.3, or in a more accurate manner by Eq.5, it is possible to evaluate indirectly the energy absorbed by a unitary surface of fracture given by the crack growth in an orthotropic material, i.e. the so called critical strain energy release rate G_{Ic}, through the following relationship [23,27]:

$$G_{Ic} = \frac{K_{Ic}^2}{\sqrt{2E_L E_T}} \sqrt{\sqrt{\frac{E_L}{E_T}} + \frac{E_L}{2G_{LT}} - \nu_{LT}} \tag{9}$$

being E_L, E_T, G_{LT} and ν_{LT} the main in-plane elastic constant of the homogeneous orthotropic material equivalent to the biocomposite laminate considered.

In order to highlight the effects of the anisotropy (represented by C_{anis}) as well as of the damage that occurs in the N-TDZ (represented by the a_{eq}), on the estimation of the fracture toughness performed through the K_{Ic} value, this has been evaluated for each laminates considered, by using first the Eq.3 as proposed by the ASTM standard with the nominal values of the crack length, and then by Eq.5 with both the nominal crack length of 26 mm (K'_{Ic}) and the equivalent crack length a_{eq} obtained through the compliance curve (K''_{Ic}). The values so obtained are shown in the following Fig.10:

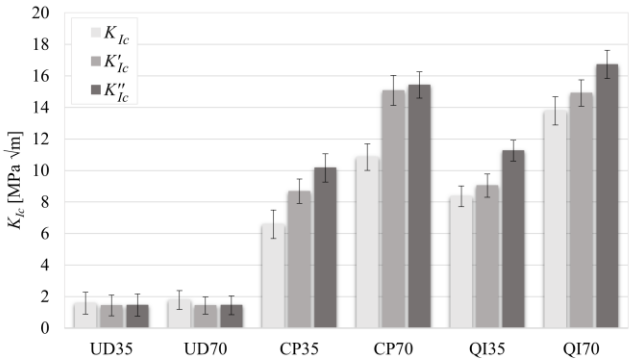

Figure 10 Values of the critical stress intensity factor obtained by using Eq.3 and Eq.5.

From the analysis of Fig.10 it is seen how for CP and QI lay-ups the values of K_{Ic} provided by Eq.3 without any correction, are always significantly less than (underestimation) the values K'_{Ic} obtained by the application of the coefficient C_{anis} by Eq.5 with $a = a_{nom}$. In turn, these last values (K'_{Ic}) are less than the values K''_{Ic} provided by Eq.5 with $a = a_{eq}$. In detail, it is seen that the correction due to the material anisotropy, corresponding to the value of C_{anis} reported in Tab.5, varies between about 8% for the QI laminates, to about 30%-40% for the CP laminates. The further correction due to the N-TDZ, instead, takes significant values especially for the laminates with V_f =35%, for which it varies from about 15% for CP35 to about 20% for QI35. Finally, except the UD laminates affected by limited corrections less than -0.5 kJ/m^2, the total correction due to the material anisotropy and the N-TDZ take significant values, up to about 55% for the CP35 laminates.

However, due to the significant extension of the N-TDZ it is necessary to assess the accuracy of the K''_{Ic} values by compare they with the estimations of the fracture toughness given by alternative energetic methods based on G_{Ic}. In order to allow such a comparison, by using the Eq.9 the corresponding values of the G''_{Ic} have been computed (see Fig.11).

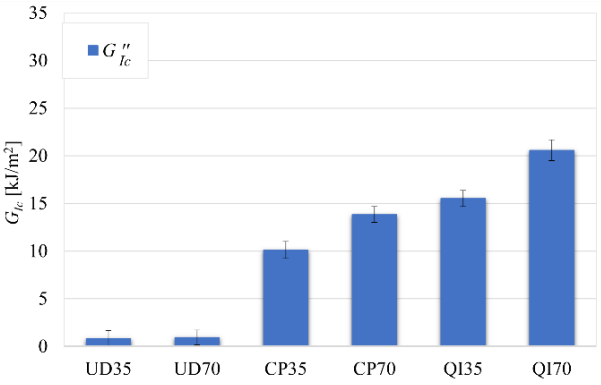

Figure 11 Values of $\boldsymbol{G''_{Ic}}$ obtained by Eq.9 from the values of $\boldsymbol{K''_{Ic}}$ obtained from Eq.5 with $a = a_{eq}$.

The analysis of Fig.11 shows in detail how also in terms of the energy necessary to the formation of a unitary surface of fracture, the LEFM approach indicates that fracture toughness of the biocomposites examined increases significantly by passing from the UD laminates to the CP laminate (up to 10 times and over), to the QI laminates (further average increments of about 50%). The redoubling of the fiber concentration that occurs from V_f = 35% to V_f = 70% instead, leads to a fracture toughness increment of about 35%. Although such a result is not in accordance with the predominant fiber failure phenomena observed experimentally, that should lead to a redouble of the fracture toughness if the fiber concentration redoubles, it is fully justified by the higher effects of the N-TDZ that occurs in the biocomposites with V_f=35%.

5.2 Critical strain energy release rate approaches

The estimation of the fracture toughness by energetic approach is based on the direct evaluation of the G_{Ic} without the use of the LEFM. As mentioned above, the so-called *Area Method* (AM) and *Compliance Calibration* (CC) [23] will be used in the following.

5.2.1 Area Method (AM)

As it is well-known, in this method the G_{Ic} value is related to the crack increment Δa that occurs from the critical load P_c, with the consequent load reduction to the final value P_e, through the following relationship obtained from the simple ratio of the energy released (equal to $^1/_2\,[(P_c - P_e)u_c - (u_e - u_c)P_e]$) and the fracture surface $t\,\Delta a$:

$$G_{Ic} = \frac{^1/_2\,[(P_c - P_e)u_c - (u_e - u_c)P_e]}{t\Delta a} = \frac{(P_c u_e - P_e u_c)}{2t\Delta a} \qquad (10)$$

In order to avoid the potential errors related to the ill-conditioning of Eq.10, the values of P_e on the fracture curves have been chosen in such a way to assure that the difference $(P_c u_e - P_e u_c)$ is always not less than 15% of the maximum value $P_c u_e$ that correspond to the complete fracture of the specimen ($P_e = 0$). The P_e values so identified for all the biocomposites examined, are depicted in Fig.5 by cyan points.

Also, it is important to note that due to the non-uniform in-depth crack growth, the direct measurement of the crack length by visual observation is a difficult task and the relative values are in general non accurate, so that the approach based on the computation of the crack length from the compliance measurement is more accurate and, at the same time, it allows the user to take into account the N-TDZ effects, as well as the fiber-bridging observed during crack propagation if the crack propagation is also considered.

In order to highlight such effects, G_{Ic} has been computed through Eq.10 by considering both the nominal crack increment Δa obtained by the visual observation by camera (AM), and the equivalent crack increment $\Delta a_{eq} = [a_{eq}(P_c) - a_{eq}(P_e)]$ calculated by Eq.1 (modified area method, MAM); the values so obtained are shown in Fig.12:

First, the comparison of the results of AM and MAM for the CP and QI laminates, shows that the effects of the N-TDZ and of the initial fiber-bridging effects lead to appreciable increments of the computed G_{Ic}, with appreciable deviations generally included between 15% and 70%.

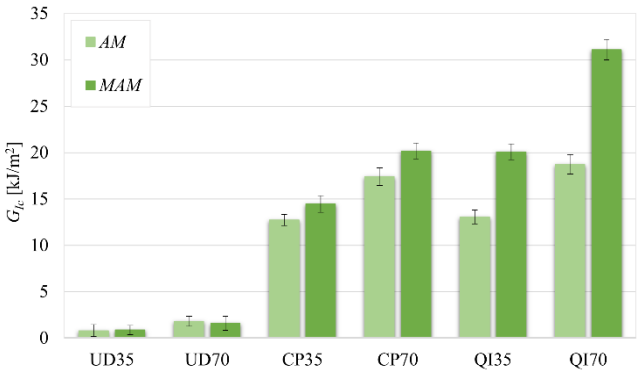

Figure 12 Values of G_{Ic} computed by AM and MAM for the various biocomposites examined.

Furthermore, in accordance with the qualitative indications provided previously by the LEFM, the fracture toughness increases significantly from UD laminates to CP laminates and hence to QI laminates, although the values now provided by MAM for the angle-ply laminates are significantly higher. Such difference can be partially justified by the beneficial fiber-bridging phenomena that occurs during crack propagation.

Finally, considering the influence of the fiber volume fraction, it can be observed that passing from V_f =35% to V_f=70% the fracture toughness increases of about 50%, i.e. it does not redoubles, confirming again the greater (positive) effects of the larger N-TDZ in the laminates with lower fiber fraction.

5.2.2 Compliance Calibration (CC)

As it is well-known from literature, in this method G_{Ic} is related to the value of the critical load and the corresponding value of the derivative of the compliance function $C(a)$ at the point identified by the critical compliance $C_c = u_c / P_c$, through the simple relationship:

$$G_{Ic} = \frac{P_c^2}{2t}\frac{dC}{da} \tag{11}$$

Also this method allows to take into account the effects of N-TDZ if the derivative is calculated rather than at the point of $C(a)$ corresponding to a_{nom} (CC), at the point corresponding to a_{eq} (Modified Compliance Calibration, MCC). Obviously, unlike the AM in which G_{Ic} is the average specific energy of the crack increment considered, the CC provides a point value of G_{Ic} at the incipient crack growth

condition (the so called “initial fracture toughness”) without take into account the successive fiber bridging phenomena that occur during crack propagation. Consequently, the comparison of MAM and MCC results, permits to highlight the effects of the fiber-bridging around the critical load. Moreover, the comparison between the results of the CC and the MCC provides an accurate assessment of the effects of the N-TDZ, without the effects of the fiber-bridging that instead are always included in the evaluation of the fracture toughness performed by MAM.

Unfortunately, respect to the AM and MAM results, the point value provided by CC and MCC are typically affected by a relatively high scattering, due also to the lower accuracy of the derivative of a function derived experimentally or by numerical simulation. For this reason the AM and MAM methods are in principle more accurate than CC and MCC methods.

However, by deriving Eq.1 with respect to a and replacing it into Eq.11, the following resolving formula is obtained:

$$G_{Ic} = \frac{P_c^2}{2t}(c_1 + 2c_2 a + 3c_3 a^2 + 4c_4 a^3 + 5c_5 a^4 + 6c_6 a^5) \qquad (12)$$

The following Fig.13 shows the G_{Ic} values evaluated by Eq.12 for each composite examined, by considering both the nominal value (CC) and the equivalent value (MCC) of the crack length.

The comparison of the results of CC and MCC reported in Fig.13, shows that for CP and QI laminates the effect of the N-TDZ is generally quite significant and it is in a very good agreement with the values of the increments $a_{eq}(P_c)$ - $a_{nom}(P_c)$ of the critical length reported in Tab.4; the percentage deviations of G_{Ic} vary in practice from about 5% for the CP70 laminates, which corresponds to the minimum value of $a_{eq}(P_c)$ - $a_{nom}(P_c)$ = 0.37 mm, up to about 55% for the QI35 laminates, which corresponds to the maximum value of $a_{eq}(P_c)$ - $a_{nom}(P_c)$ = 3.30 mm. This fully confirms that the effects of the N-TDZ cannot be neglected for an accurate analysis of the fracture toughness of the biocomposites considered.

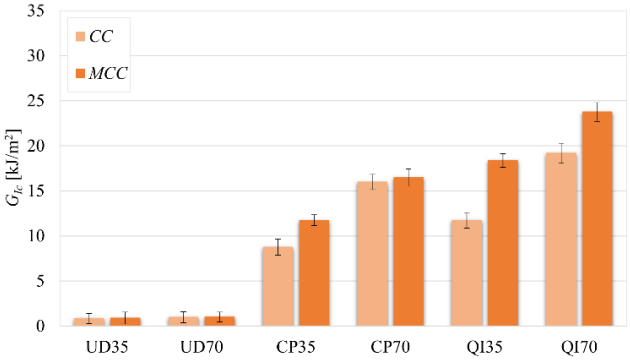

Figure 13 Values of G_{Ic} evaluated by the CC and the MCC for the biocomposites examined.

5.3 Comparative analysis and accuracy estimations

The following Fig.14 shown the comparison between the values of G_{Ic} evaluated with the corrected LEFM (i.e. by Eq.5 with $a = a_{eq}$) and with MAM and MCC.

As discussed in section 5.2, the comparison between the results of the MAM and the MCC shown in Fig.14 allows to highlight the effects of fiber bridging that occur surrounding the critical load (incipient crack growth): they are negligible only for UD35, whereas they lead to appreciable percentage

increments of the fracture toughness for all other laminates, with values ranging from about 11% for QI35 (minimum value) to about 31% for QI70 (maximum value).

The comparison of the LEFM results with the MCC results (both point methods that do not take into account the fiber bridging effects) confirms instead that, due to the significant extension of the N-TDZ respect to the SDZ, the LEFM underestimates the actual fracture toughness of the examined laminates, with errors ranging from about 8% for the UD laminates to about 18% for the CP ones, to about 20%-30% for the QI ones. Taking into account also the effects of bridging, i.e. by comparing the results of the LEFM with those of the MAM, it is detected errors ranging from about 30% for the UD and the QI laminates to about 45% for the CP ones. Therefore, it is possible to state that for the biocomposites examined the fracture toughness cannot be accurately evaluated by LEFM, but only through energetic methods; between them, the MAM is the most accurate because it takes into account not only the effects of the N-DTZ but also the significant bridging-effects that occur when the crack start to propagate around the critical load.

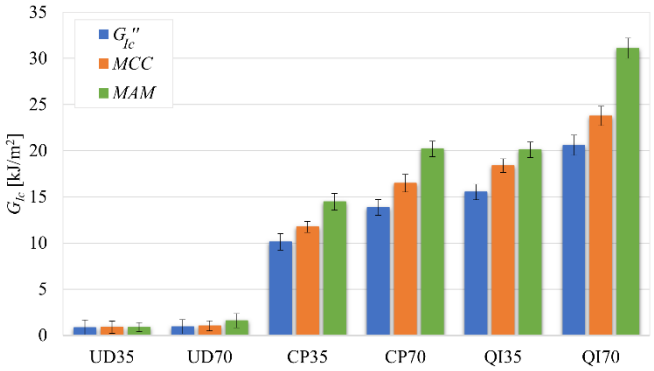

Figure 14 Values of G_{Ic} provided by LEFM, MAM and MMC for the biocomposites examined.

5.4 Analysis of the resistance *R-curves*

The experimental evidence shows that in the biocomposite laminates analyzed the effects of fiber bridging tend to increase appreciably with the progressive crack growth, reaching a stable condition after a crack growth of about 8-10 mm; also, the crack growth tends to become instable only after this fiber bridging stabilization. Consequently, it is possible to state that the examined biocomposite exhibit significant *R-curves* whose asymptotic values constitute the true fracture toughness that is in general appreciable higher than the initial fracture toughness above determined.

In order to evaluate this material property, the evolution of G_{Ic} with the progressive crack growth (*R-curves*) have been computed by using the MAM; the relative results are reported in the following Fig.15.

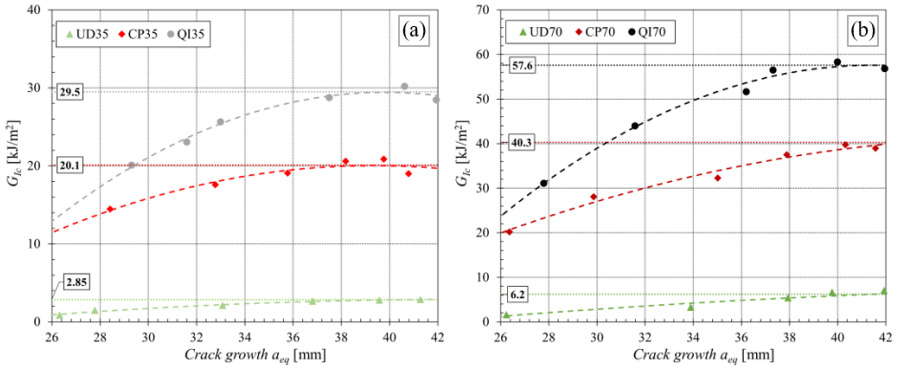

Figure 15 *R-curves* obtained by using MAM for the biocomposites having (a) V_f = 35% and (b) V_f = 70%.

As expected, Fig.15 shows that for all the laminates the G_{Ic} values increases significantly with the crack growth; the asymptotic values correspond to significant increments (respect the initial ones) up to about 100% and 240% respectively for CP and QI laminates, fully confirming that the effects of fiber bridging contribute in a very robust manner to the fracture toughness of the biocomposites examined. The higher fiber-bridging effects of the laminae at ±45° with respect to 0° and 90° laminae, justifies the higher increments observed for the QI laminates. Finally, it is very interesting to observe how the asymptotic values obtained for the different laminates are in practice proportional to the fibre volume fraction: moving from laminates with V_f = 35% (Fig.15a) to laminates with V_f = 70% (Fig.15b) G_{Ic} passes from values of 2.85 kJ/m^2, 20.1 kJ/m^2 and 29.5 kJ/m^2 to values almost double of 6.2 kJ/m^2, 40.3 kJ/m^2 and 57.6 kJ/m^2, respectively for UD, CP and QI laminates.

5.5 Specific critical energy strain rate and laminate lay-up optimization

In accordance with the experimental evidence above illustrated in detail, it is possible to state that the fracture toughness of a generic biocomposite laminate type $[0_\alpha/90_\beta/\pm45_\gamma]_S$ is essentially linked to V_f as well as to the particular lay-up defined by the percentages α, β e γ of laminae placed at 0°, 90° e ±45° respectively. In particular, since the damage mechanisms of each lamina (fiber and matrix tensile failure for the 0° laminae, matrix delamination and limited fiber shear failure for the 90° laminae, fiber and matrix shear failure for ±45° laminae) are in practice independent of the particular laminate lay-up, then for the generic laminate univocally identified by the quatern (α, β, γ, V_f) the asymptotic value of G_{Ic} can be evaluated at the design stage by the following linear relationship:

$$G_{Ic}(\alpha,\beta,\gamma,V_f) = G_{Ic}^{0}(V_f)\,\alpha + \; G_{Ic}^{90}(V_f)\,\beta + G_{Ic}^{\pm45}(V_f)\,\gamma \tag{13}$$

being $G_{Ic}^{0}(V_f)$, $G_{Ic}^{90}(V_f)$ and $G_{Ic}^{\pm45}(V_f)$ respectively the specific fracture energy of the lamina placed at 0°, 90° and ±45°, having fibre volume concentration equal to V_f.

In detail, by applying Eq.13 to the CP35 and CP70 laminates examined, the unknown values $G_{Ic}^{0}(35\%)$, $G_{Ic}^{0}(70\%)$ are immediately evaluated from the following equation system (numerical values taken from Fig.15):

$$G_{Ic}(0.5,0.5,0,35\%) = G_{Ic}^{0}(35\%)\cdot 0.5 + 2.85\cdot 0.5 = 20.1 \text{ kJ/m}^2 \tag{14}$$

$$G_{Ic}(0.5,0.5,0,70\%) = G_{Ic}^{0}(70\%)\cdot 0.5 + \; 6.2\cdot 0.5 = 40.3 \text{ kJ/m}^2 \tag{15}$$

By solving this, it follows:

$$G_{Ic}^{0}(35\%) = 37.4 \text{ kJ/m}^2 \; \textit{and} \; G_{Ic}^{0}(70\%) = 74.4 \text{ kJ/m}^2$$

Similarly, the values of $G_{Ic}^{\pm45}(35\%)$ and $G_{Ic}^{\pm45}(70\%)$ ·can be estimated by applying Eq.13 to QI35 and QI70 laminates (numerical values taken again from Fig.15):

$$G_{Ic}(0.25,0.25,0.50,35\%) = 37.4\,0.25 + 2.85\cdot 0.25 + G_{Ic}^{\pm45}(35\%)\cdot 0.50 = 29.5 \text{ kJ/m}^2 \tag{16}$$

$$G_{Ic}(0.25,0.25,0.50,70\%) = 74.4\cdot 0.25 + \; 6.2\cdot 0.25 + G_{Ic}^{\pm45}(70\%)\cdot 0.50 = 57.6 \text{ kJ/m}^2 \tag{17}$$

By solving Eqs.16 and 17 it follows:

$$G_{Ic}^{\pm 45}(35\%) = 38.9 \text{ kJ/m}^2 \quad \text{and} \quad G_{Ic}^{0}(70\%) = 74.9 \text{ kJ/m}^2$$

The following Tab.6 summarizes the above calculated asymptotic G_{Ic} values of single unidirectional lamina by varying V_f as well as its relative orientation (0°, 90°, ±45°):

Table 6 Asymptotic G_{Ic} values for the single unidirectional lamina.

V_f	G_{Ic}^{90} [kJ/m^2]	$G_{Ic}^{\pm 45}$ [kJ/m^2]	G_{Ic}^{0} [kJ/m^2]
35%	2.85	38.9	37.4
70%	6.2	74.9	74.4

The analysis of Tab.6 shows that the contribution of a lamina at 90° to the fracture toughness of the laminate, is relatively small (about 3÷6 kJ/m^2) whereas the significant contributions are given by the laminae at 0° or ±45°, that exhibit comparable values of fracture energy of about 38 kJ/m^2 and 75 kJ/m^2 for V_f =35% and V_f =70% respectively. Consequently, the substitution of laminae oriented at 0° with laminae oriented at ±45° does not lead to significant changes of the fracture toughness of the laminate; also, to maximize the fracture toughness of a laminate having fixed values of V_f and thickness, it is necessary to avoid the use of laminae at 90° (i.e. to use laminates with β=0), by fixing the percentage of laminae at 0° and at ±45° as a function of the magnitude of the tensile (laminae at 0°) and shear (laminae at 45°) loads actually applied. In other words, the best lay-up of biocomposites laminates for structural and semi-structural applications subject to high fracture risks is $[0_\alpha/\pm 45_{1-\alpha}]_S$ with V_f =70%, which corresponds a fracture toughness of 75 kJ/m^2.

Finally, as observed in the previous section about the proportionality of the fracture energy to the fiber volume concentration V_f, it can be stated that the toughness $G_{Ic}^{\theta}(V_f)$ of a generic unidirectional lamina having fiber volume concentration V_f and orientation θ = 0°, 90° or ±45°, can be determined by using Tab.6 data through the simple linear relationship:

$$G_{Ic}^{\theta}(V_f) = G_{Ic}^{\theta}(35\%) + [G_{Ic}^{\theta}(70\%) - G_{Ic}^{\theta}(35\%)](V_f - 35\%)/35\% \qquad (18)$$

In order to assess the indications above obtained about the optimal lay-up as well as the accuracy of both Eq.18 and Eq.13, three biocomposites having optimized lay-up $[0_\alpha/\pm 45_{1-\alpha}]_S$ (with α=1/3) and intermediate fiber fraction V_f =50%, have been manufactured and subjected to fracture tests. In the following Tab.7 the relative fracture toughness obtained experimentally by MAM, are compared with the values provided by the use of Eq.18 and Eq.13 (α=1/3, β=0, γ=2/3):

Table 7 Fracture test results of several biocomposites with optimized lay-up.

Lay-up	V_f [%]	**thickness** [mm]	G_{Ic} from Eqs.18 and 13 [kJ/m^2]	G_{Ic} given by MAM [kJ/m^2]	**Deviation** [%]
$[0/\pm 45]_S$	50	1.5	56.6	**61.9**	+9.4
$[0_2/(\pm 45)_2]_S$	50	3.0	56.6	**56.1**	-1.0
$[0_3/(\pm 45)_3]_S$	50	4.5	56.6	**52.2**	-8.8

The analysis of the deviations between the experimental results and the value predicted by Eq.18 and 13 show a good accuracy; in detail, the correlation between the sign of the deviations and the laminate

thickness highlight that, as it is widely shown in literature, the fracture toughness of the laminate tends to decrease when the laminate thickness increases. However, in the range 1.5 – 4.5 mm of practical application of the examined laminates, such variation is in general included in the range ±10%.

6 COMPARISON WITH OTHER LITERATURE RESULTS

Taking into account that composites and biocomposites are essentially materials used in *light-weight* applications where the relevant characteristic parameter is the specific one, obtained by dividing the absolute parameter by the specific weight, in the following the comparison between the fracture toughness of the biocomposites examined and that of other materials is then carried out by considering the specific energy G_{Ic}/ρ being ρ the specific weight (see Fig.16).

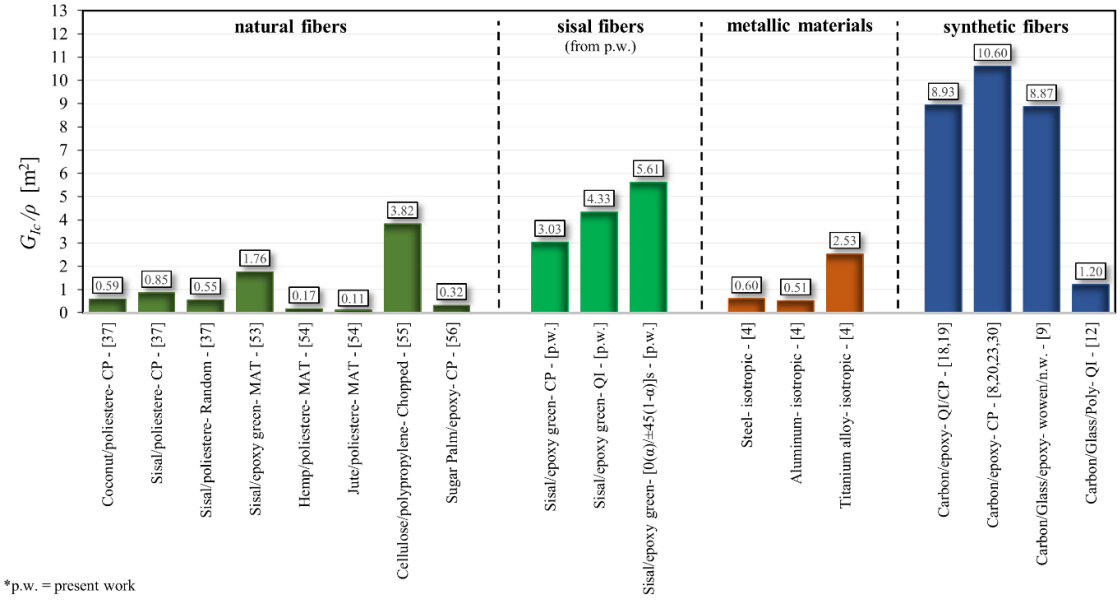

Figure 16 Specific energy G_{Ic}/ρ for different composites, biocomposites and metallic materials.

Fig.16 shows that the high performance biocomposites examined in this work can reach specific fracture toughness G_{Ic}/ρ up to 5.61 m^2 (optimized lay-ups without laminae at 90°). This value is about 35% ÷ 45% lower than that of performing and relatively much more expensive synthetic CFRP or hybrids GCFRP, which exhibit specific toughness values in the range 8.87 to 10.6 m^2. The comparison with traditional metal materials such as steel and aluminum, which exhibit G_{Ic}/ρ values included in the range 0.5-0.6 m^2, shows how the examined biocomposites have a fracture toughness 5-10 times higher. Also, it is 4-10 times higher than other biocomposites reinforced by natural fibers reported in literature, having specific toughness ranging from 0.55 to 0.85 m^2. Finally, the biocomposites examined have specific fracture toughness also higher than titanium and its alloys (very appreciated in the fracture field for the high K_{Ic} values exhibited) that have specific resistance in the order of 2.5 m^2.

Consequently it can be said that in terms of specific fracture toughness the high performance biocomposites examined are appreciable more performing respect not only to similar biocomposites developed and studied in the literature, but also to traditional metal materials such as steel, aluminum

and titanium alloys, that therefore can be replaced by these biocomposites even for applications characterized by high fracture risks. Also, the substitution of high performance synthetic composites (CFRP, GCFRP etc.) can be reasonably considered too, if the significant advantages offered by the examined biocomposites in terms of eco-compatibility and cost (that is in general lower than one order of magnitude), are properly considered.

7 CONCLUSIONS

The experimental analysis of the translaminar fracture toughness of high performance biocomposite laminates reinforced by sisal fibers, by varying the fiber volume concentration V_f and the lay-up, have allowed to show that:

- although an appropriate corrective function that takes into account the anisotropy of the examined biocomposites has been introduced by the authors and the effects of the local damage of the material near the crack tip is properly considered by using the so called equivalent crack length, the LEFM does not provide accurate estimations even for the initial fracture toughness, mainly because the extension of the damaged area near the crack tip is higher than that of the singular dominate zone.
- accurate values of initial G_{Ic} are instead provided by the proposed modified area method, that take into account the effects of the local damage of the material through the equivalent crack length. The use of the modified compliance calibration method provides instead approximated results, because it does not consider the effects of significant fiber-bridging that occur when the crack start to propagate from the critical load.
- the analysis of the damage mechanisms observed for the different unidirectional, cross-ply and quasi-isotropic laminates, have shown that these involve respectively the intralaminar delamination of the laminae at 90°, the tensile failure fibers and matrix of the laminae at 0° and the shear failure of fibers and matrix of the laminae at ±45°; moreover, the crack propagation is followed by significant and progressive fiber-bridging phenomena that lead to noticeable increments of the fracture toughness, that stabilizes after about 8-10 mm of crack growth. These asymptotic values obtained by appropriate *R*-curves analysis, constitutes the true fracture toughness of the biocomposites examined.
- also, the analysis of the various lay-ups considered (with V_f =35% and 70%) have allowed to detect that the specific fracture energy of the unidirectional lamina oriented at 0° (aligned with the load), at 90° and ±45°, is always proportional to the fibre volume fraction and therefore, the corresponding fracture energy values computed in the present work (2.85, 37.4 and 38.9 kJ/m2 for V_f =35% and 6.2, 74.4 and 74.9 for V_f =70%) allow the designer to predict the fracture toughness of a laminate with a generic lay-up, as the sum of the contributions of the individual laminae, obtained by simple linear interpolation with respect to V_f.

- the comparison with other materials reported in literature, have shown that the examined biocomposites have specific fracture toughness G_{Ic}/ρ that is about 35% ÷ 45% lower than those of expensive CFRP and hybrid GCFRP properly implemented. Also, it is significantly higher than that of both other biocomposites reinforced by natural fibers (jute, hemp, etc.), and traditional metal materials such as steel, aluminum and titanium; therefore, these last materials can be replaced advantageously by the analyzed eco-friendly biocomposites, also of structural components subjected to high fracture risks. Thanks to the low cost of the sisal fibers, such substitutions would lead not only to a reduction of the environmental impact, but also to an interesting cost reduction.

ACKNOWLEDGEMENTS

The authors gratefully acknowledge the financial support of the open access funding provided by University of Palermo.

REFERENCES

[1] F. Ahmad, H.S. Choi, M.K. Park, A review: Natural fiber composites selection in view of mechanical, light weight, and economic properties, Macromol. Mater. Eng. 300 (2015) 10–24. https://doi.org/10.1002/mame.201400089.

[2] G. Koronis, A. Silva, M. Fontul, Green composites: A review of adequate materials for automotive applications, Compos. Part B Eng. 44 (2013) 120–127. https://doi.org/10.1016/j.compositesb.2012.07.004.

[3] K.L. Pickering, M.G.A. Efendy, T.M. Le, A review of recent developments in natural fibre composites and their mechanical performance, Compos. Part A Appl. Sci. Manuf. 83 (2016) 98–112. https://doi.org/10.1016/j.compositesa.2015.08.038.

[4] A.J. Brunner, Fracture mechanics of polymer composites in aerospace applications, Elsevier Ltd, 2020. https://doi.org/10.1016/b978-0-08-102679-3.00008-3.

[5] Tada H; Paris PC; Irwin GR., The stress analysis of cracks handbook, 2000.

[6] M.J. Laffan, S.T. Pinho, P. Robinson, A.J. McMillan, Translaminar fracture toughness testing of composites: A review, Polym. Test. 31 (2012) 481–489. https://doi.org/10.1016/j.polymertesting.2012.01.002.

[7] K. Allaer, I. De Baere, W. Van Paepegem, J. Degrieck, Direct fracture toughness determination of a ductile epoxy polymer from digital image correlation measurements on a single edge notched bending sample, Polym. Test. 42 (2015) 199–207. https://doi.org/10.1016/j.polymertesting.2015.01.014.

[8] G. Catalanotti, P.P. Camanho, J. Xavier, C.G. Dávila, A.T. Marques, Measurement of resistance curves in the longitudinal failure of composites using digital image correlation, Compos. Sci. Technol. 70 (2010) 1986–1993. https://doi.org/10.1016/j.compscitech.2010.07.022.

[9] A. Ortega, P. Maimí, E. V. González, J.R. Sainz de Aja, F.M. de la Escalera, P. Cruz, Translaminar fracture toughness of interply hybrid laminates under tensile and compressive loads, Compos. Sci. Technol. 143 (2017) 1–12. https://doi.org/10.1016/j.compscitech.2017.02.029.

[10] D. Flore, B. Stampfer, K. Wegener, Experimental and numerical failure analysis of notched quasi-unidirectional laminates at room temperature and elevated temperature, Compos. Struct. 160 (2017) 128–141. https://doi.org/10.1016/j.compstruct.2016.10.046.

[11] B. Vieille, M. Chabchoub, C. Gautrelet, Influence of matrix ductility and toughness on strain energy release rate and failure behavior of woven-ply reinforced thermoplastic structures at high temperature, Compos. Part B Eng. 132 (2018) 125–140. https://doi.org/10.1016/j.compositesb.2017.08.011.

[12] B. Vieille, J.D. Gonzalez, C. Bouvet, Fracture mechanics of hybrid composites with ductile matrix and brittle fibers: Influence of temperature and constraint effect, J. Compos. Mater. 53 (2019) 1361–1376. https://doi.org/10.1177/0021998318802613.

[13] B. Vieille, Evolution of the strain energy release rate during ductile or brittle failure in woven-ply reinforced thermoplastic laminates under high temperature conditions, Polym. Compos. 40 (2019) 121–131. https://doi.org/10.1002/pc.24612.

[14] D. Dalli, G. Catalanotti, L.F. Varandas, B.G. Falzon, S. Foster, Mode I intralaminar fracture toughness of 2D woven carbon fibre reinforced composites: A comparison of stable and unstable crack propagation techniques, Eng. Fract. Mech. 214 (2019) 427–448. https://doi.org/10.1016/j.engfracmech.2019.04.003.

[15] G. Catalanotti, A. Arteiro, M. Hayati, P.P. Camanho, Determination of the mode I crack resistance curve of polymer composites using the size-effect law, Eng. Fract. Mech. 118 (2014) 49–65. https://doi.org/10.1016/j.engfracmech.2013.10.021.

[16] M. V. Donadon, B.G. Falzon, L. Iannucci, J.M. Hodgkinson, Intralaminar toughness characterisation of unbalanced hybrid plain weave laminates, Compos. Part A Appl. Sci. Manuf. 38 (2007) 1597–1611. https://doi.org/10.1016/j.compositesa.2006.12.003.

[17] T. Lisle, M.L. Pastor, C. Bouvet, P. Margueres, Damage of woven composite under translaminar cracking tests using infrared thermography, Compos. Struct. 161 (2017) 275–286. https://doi.org/10.1016/j.compstruct.2016.11.030.

[18] R.F. Teixeira, S.T. Pinho, P. Robinson, Translaminar fracture toughness of CFRP: From the toughness of individual plies to the toughness of the laminates, ECCM 2012 - Compos. Venice, Proc. 15th Eur. Conf. Compos. Mater. (2012) 24–28.

[19] R.F. Teixeira, S.T. Pinho, P. Robinson, Translaminar ply fracture toughness of advanced composites, ICCM Int. Conf. Compos. Mater. (2011) 1–6.

[20] M.J. Laffan, S.T. Pinho, P. Robinson, A.J. McMillan, Translaminar fracture toughness: The critical notch tip radius of 0° plies in CFRP, Compos. Sci. Technol. 72 (2011) 97–102. https://doi.org/10.1016/j.compscitech.2011.10.006.

[21] E.A. Papon, A. Haque, Fracture toughness of additively manufactured carbon fiber reinforced composites, Addit. Manuf. 26 (2019) 41–52. https://doi.org/10.1016/j.addma.2018.12.010.

[22] H.E. Balcıoğlu, D. Yalçın, The Determination of Fracture Characterization of Knitted Fabric Reinforced Composites Using Arcan Test, Fibers Polym. 21 (2020) 849–863. https://doi.org/10.1007/s12221-020-9619-z.

[23] M.J. Laffan, S.T. Pinho, P. Robinson, L. Iannucci, Measurement of the in situ ply fracture toughness associated with mode I fibre tensile failure in FRP. Part I: Data reduction, Compos. Sci. Technol. 70 (2010) 606–613. https://doi.org/10.1016/j.compscitech.2009.12.016.

[24] G. Bullegas, J. Moledo Lamela, S. Pimenta, S. Taveira Pinho, On the role of dynamic stress concentrations and fracture mechanics in the longitudinal tensile failure of fibre-reinforced composites, Eng. Fract. Mech. 228 (2020) 106920. https://doi.org/10.1016/j.engfracmech.2020.106920.

[25] A. Thionnet, From Fracture to Damage Mechanics: A behavior law for microcracked composites using the concept of Crack Opening Mode, Compos. Struct. 92 (2010) 780–794. https://doi.org/10.1016/j.compstruct.2009.08.047.

[26] M. Fakoor, S. Shahsavar, Fracture assessment of cracked composite materials: Progress in models and criteria, Theor. Appl. Fract. Mech. 105 (2020) 102430. https://doi.org/10.1016/j.tafmec.2019.102430.

[27] D. Dalli, G. Catalanotti, L.F. Varandas, B.G. Falzon, S. Foster, Compressive intralaminar fracture toughness and residual strength of 2D woven carbon fibre reinforced composites: New developments on using the size effect method, Theor. Appl. Fract. Mech. 106 (2020) 102487. https://doi.org/10.1016/j.tafmec.2020.102487.

[28] G. Catalanotti, J. Xavier, P.P. Camanho, Measurement of the compressive crack resistance curve of composites using the size effect law, Compos. Part A Appl. Sci. Manuf. 56 (2014) 300–307. https://doi.org/10.1016/j.compositesa.2013.10.017.

[29] P. Kuhn, G. Catalanotti, J. Xavier, M. Ploeckl, H. Koerber, Determination of the crack resistance curve for intralaminar fiber tensile failure mode in polymer composites under high rate loading, Compos. Struct. 204 (2018) 276–287. https://doi.org/10.1016/j.compstruct.2018.07.039.

[30] S.T. Pinho, P. Robinson, L. Iannucci, Fracture toughness of the tensile and compressive fibre failure modes in laminated composites, Compos. Sci. Technol. 66 (2006) 2069–2079. https://doi.org/10.1016/j.compscitech.2005.12.023.

[31] S. Ko, J. Davey, S. Douglass, J. Yang, M.E. Tuttle, M. Salviato, Effect of the thickness on the fracturing behavior of discontinuous fiber composite structures, Compos. Part A Appl. Sci. Manuf. 125 (2019) 105520. https://doi.org/10.1016/j.compositesa.2019.105520.

[32] M. Salviato, K. Kirane, S. Esna Ashari, Z.P. Bažant, G. Cusatis, Experimental and numerical investigation of intra-laminar energy dissipation and size effect in two-dimensional textile composites, Compos. Sci. Technol. 135 (2016) 67–75. https://doi.org/10.1016/j.compscitech.2016.08.021.

[33] A. Arteiro, C. Furtado, G. Catalanotti, P. Linde, P.P. Camanho, Thin-ply polymer composite materials: A review, Compos. Part A Appl. Sci. Manuf. 132 (2020). https://doi.org/10.1016/j.compositesa.2020.105777.

[34] G. Catalanotti, P. Kuhn, J. Xavier, H. Koerber, High strain rate characterisation of intralaminar fracture toughness of GFRPs for longitudinal tension and compression failure, Compos. Struct. 240 (2020) 112068. https://doi.org/10.1016/j.compstruct.2020.112068.

[35] J.M.L. Reis, Sisal fiber polymer mortar composites: Introductory fracture mechanics approach, Constr. Build. Mater. 37 (2012) 177–180. https://doi.org/10.1016/j.conbuildmat.2012.07.088.

[36] B. Tiber, H.E. Balcıoğlu, Flexural and fracture behavior of natural fiber knitted fabric reinforced composites, Polym. Compos. 40 (2019) 217–228. https://doi.org/10.1002/pc.24635.

[37] R. V. Silva, D. Spinelli, W.W. Bose Filho, S. Claro Neto, G.O. Chierice, J.R. Tarpani, Fracture toughness of natural fibers/castor oil polyurethane composites, Compos. Sci. Technol. 66 (2006) 1328–1335. https://doi.org/10.1016/j.compscitech.2005.10.012.

[38] S. Keck, M. Fulland, Effect of fibre volume fraction and fibre direction on crack paths in unidirectional flax fibre-reinforced epoxy composites under static loading, Theor. Appl. Fract. Mech. 101 (2019) 162–168. https://doi.org/10.1016/j.tafmec.2019.01.028.

[39] B. Zuccarello, R. Scaffaro, Experimental analysis and micromechanical models of high performance renewable agave reinforced biocomposites, Compos. Part B Eng. 119 (2017) 141–152. https://doi.org/10.1016/j.compositesb.2017.03.056.

[40] B. Zuccarello, G. Marannano, Random short sisal fiber biocomposites: Optimal manufacturing process and reliable theoretical models, Mater. Des. 149 (2018) 87–100. https://doi.org/10.1016/j.matdes.2018.03.070.

[41] B. Zuccarello, G. Marannano, A. Mancino, Optimal manufacturing and mechanical characterization of high performance biocomposites reinforced by sisal fibers, Compos. Struct. 194 (2018) 575–583. https://doi.org/10.1016/j.compstruct.2018.04.007.

[42] B. Zuccarello, M. Zingales, Toward high performance renewable agave reinforced biocomposites: Optimization of fiber performance and fiber-matrix adhesion analysis, Compos. Part B Eng. 122 (2017) 109–120. https://doi.org/10.1016/j.compositesb.2017.04.011.

[43] B. Zuccarello, G. Marannano, F. Bongiorno, Resistenza statica e a fatica di nuovi laminati biocompositi rinforzati con fibre di agave, in: 47° ASIAS Natl. Conf., Reggio Calabria, 2018.

[44] C. Militello, F. Bongiorno, G. Epasto, B. Zuccarello, Low-velocity impact behaviour of green epoxy biocomposite laminates reinforced by sisal fibers, Compos. Struct. 253 (2020) 112744. https://doi.org/10.1016/j.compstruct.2020.112744.

[45] B. Zuccarello, M. Bartoli, F. Bongiorno, C. Militello, A. Tagliaferro, A. Pantano, New concept in bioderived composites: Biochar as toughening agent for improving performances and durability of agave-based epoxy biocomposites, PolymersPolymers. 13 (2021) 1–14. https://doi.org/10.3390/polym13020198.

[46] ASTM D3822 Standard Test Method for Tensile Properties of Single Textile Fibers, 2007.

[47] U. Entropy Resin Inc. (CA), Technical Data Sheet SUPER SAP ® CLR Epoxy System, n.d.

[48] ASTM E1922 Standard Test Method for Translaminar Fracture Toughness of Laminated Polymer Matrix Composite Materials, 1997.

[49] ASTM E399 Standard Test Method for Plane-Strain Fracture Toughness of Metallic Materials 1, 1997.

[50] ASTM E1820 Standard Test Method for Measurement of Fracture Toughness, 2011.

[51] ASTM D5045 Standard Test Methods for Plane-Strain Fracture Toughness and Strain Energy Release of Plastic Materials, 2007.

[52] P.O. Judt, J.C. Zarges, A. Ricoeur, H.P. Heim, Anisotropic fracture properties and crack path prediction in glass and cellulose fiber reinforced composites, Eng. Fract. Mech. 188 (2018) 344–360. https://doi.org/10.1016/j.engfracmech.2017.08.027.

[53] B. Zuccarello, C. Militello, F. Bongiorno, Influence of the anisotropy of sisal fibers on the mechanical properties of high performance unidirectional biocomposite lamina and micromechanical models, Compos. Part A Appl. Sci. Manuf. 143 (2021) 106320. https://doi.org/10.1016/j.compositesa.2021.106320.

[54] T. Alam, M.K. Gupta, R.K. Srivastava, H. Singh, Thermal Characterization and Fracture Toughness of Sisal Fiber Reinforced Polymer Composite, Int. J. Sci. Eng. Technol. 3 (2014) 1071–1073.

[55] M. Hughes, C.A.S. Hill, J.R.B. Hague, The fracture toughness of bast fibre reinforced polyester composites: Part 1 Evaluation and analysis, J. Mater. Sci. 37 (2002) 4669–4676. https://doi.org/10.1023/A:1020621020862.

[56] P. Ali khudhur, O.S. Zaroog, B.A. Khidhir, Z.S. Radif, Fracture Toughness of Sugar Palm Fiber Reinforced Epoxy Composites, Int. J. Sci. Res. 2 (2013) 273–279.

Declaration of interests

☒ The authors declare that they have no known competing financial interests or personal relationships that could have appeared to influence the work reported in this paper.

☐The authors declare the following financial interests/personal relationships which may be considered as potential competing interests:

CRediT authorship contribution statement

Francesco Bongiorno: Investigation, Data Curation, Validation, Visualization, Conceptualization, Writing - Original Draft. **Carmelo Militello**: Investigation, Data Curation, Formal analysis, Validation, Conceptualization, Writing - Original Draft. **Bernardo Zuccarello**: Term, Conceptualization, Methodology, Validation, Project administration, Writing - Review & Editing.

FIGURE CAPTIONS

Figure 1 (a) stretched and aligned fibers, (b) unidirectional "stitched" fabrics obtained in laboratory.

Figure 2 Laminates type (a) UD70, (b) CP70, (c) BP70 e (d) QI70 obtained by compression-moulding.

Figure 3 (a) sketch of the CT specimen and (b) relative specimen type CP70.

Figure 4 Specimens with V_f =70% during test and zoom of the relative fracture surfaces after test.

Figure 5 Mean fracture curves of the various biocomposite laminates considered.

Figure 6 Compliance curves obtained experimentally for the (a) UD, (b) CP and (c) QI biocomposite laminates having V_f =35% and 70%.

Figure 7 Comparison between a_{eq} and the corresponding value a_{nom} for the various examined biocomposites.

Figure 8 Comparison between the actual opening stress σ_y computed by FEM and the theoretical one for the QI70 biocomposite examined.

Figure 9 Correction coefficient C_{anis} versus the two anisotropic ratios R_E and R_G.

Figure 10 Values of the critical stress intensity factor obtained by using Eq.3 and Eq.5.

Figure 11 Values of GIc'' obtained by Eq.9 from the values of KIc'' obtained from Eq.5 with $a = a_{eq}$.

Figure 12 Values of G_{Ic} computed by AM and MAM for the various biocomposites examined.

Figure 13 Values of G_{Ic} evaluated by the CC and the MCC for the biocomposites examined.

Figure 14 Values of G_{Ic} provided by LEFM, MAM and MMC for the biocomposites examined.

Figure 15 *R-curves* obtained by using MAM for the biocomposites having (a) V_f = 35% and (b) V_f = 70%.

Figure 16 Specific energy G_{Ic}/ρ for different composites, biocomposites and metallic materials.

TABLE CAPTIONS

Table 1 Properties of the sisal fibers considerate in the present study.

Table 2 Properties of the green epoxy resin, used as matrix [47].

Table 3 Lay-up and fiber volume fraction of the various biocomposites considered.

Table 4 Values of Cc, aeq and (aeq - anom) for the various examined biocomposites.

Table 5 Coefficient Canis for the biocomposites examined.

Table 6 Asymptotic GIc values for the single unidirectional lamina.

Table 7 Fracture test results of several biocomposites with optimized lay-up.